

28 May 2010, 2:00 pm - 3:30 pm

## Effects of Internal Gas Explosion on an Underwater Tunnel Roof

Omar Al-Farouk Salem Al-Damluji  
*University of Baghdad, Iraq*

Akram Younis Thannon Al-Sa'aty  
*University of Mosul, Iraq*

Rafi' Mahmoud Sulaiman Al-Nu'aimy  
*University of Baghdad, Iraq*

Follow this and additional works at: <https://scholarsmine.mst.edu/icrageesd>



Part of the [Geotechnical Engineering Commons](#)

---

### Recommended Citation

Al-Damluji, Omar Al-Farouk Salem; Al-Sa'aty, Akram Younis Thannon; and Al-Nu'aimy, Rafi' Mahmoud Sulaiman, "Effects of Internal Gas Explosion on an Underwater Tunnel Roof" (2010). *International Conferences on Recent Advances in Geotechnical Earthquake Engineering and Soil Dynamics*. 7. <https://scholarsmine.mst.edu/icrageesd/05icrageesd/session06/7>



This work is licensed under a [Creative Commons Attribution-Noncommercial-No Derivative Works 4.0 License](#).

This Article - Conference proceedings is brought to you for free and open access by Scholars' Mine. It has been accepted for inclusion in International Conferences on Recent Advances in Geotechnical Earthquake Engineering and Soil Dynamics by an authorized administrator of Scholars' Mine. This work is protected by U. S. Copyright Law. Unauthorized use including reproduction for redistribution requires the permission of the copyright holder. For more information, please contact [scholarsmine@mst.edu](mailto:scholarsmine@mst.edu).



Fifth International Conference on

## Recent Advances in Geotechnical Earthquake Engineering and Soil Dynamics and Symposium in Honor of Professor I.M. Idriss

May 24-29, 2010 • San Diego, California

### EFFECTS OF INTERNAL GAS EXPLOSION ON AN UNDERWATER TUNNEL ROOF

**Omar Al-Farouk Salem Al-Damluji**  
Department of Civil Engineering,  
University of Baghdad, Iraq.

**Akram Younis Thannon Al-Sa'aty**  
Department of Architecture,  
University of Mosul, Iraq.

**Rafi' Mahmoud Sulaiman Al-Nu'aimy**  
Department of Civil Engineering,  
University of Baghdad, Iraq.

#### ABSTRACT

An underwater reinforced concrete tunnel roof is subjected to an internal gas explosion. Dynamic analyses are performed for three cases, namely, (1) an uncoupled solution, (2) class II coupling analysis and (3) full model with class I and II couplings. Three load cases are considered, dead (gravity) load, uniformly distributed vertical loads from sand and water and finally an internal pressure gas explosion. Linear and non-linear constitutive relationships are considered for the materials constituting the gas explosion problem. Results include time deflection of tunnel roof, time histories of stresses in vertical reinforcing bars and contours of concrete stresses for tunnel roof. By conducting analyses from various models, the question whether the tunnel would be damaged to such an extent that its serviceability would be impaired is investigated.

#### INTRODUCTION

Many types of large and complex structures have to be designed safely against blast effects. Explosions even from small charges when placed close to a structure would result in huge peak pressures and could lead to damage. Although considerable effort has been directed to the evolution of blast-resistant shelters, very little information is available on the possibility of designing ordinary residential/ commercial reinforced concrete buildings against the blast loading to provide specified margins of safety at affordable cost. Therefore, the knowledge of structural response under blast loading is increasingly important in military and civil applications. The interaction between the soil and the fluid has to be included in the analysis of structures such as dams, tanks, elevated water tanks, offshore structures, towers surrounded by water, etc.

Out of all the works done in the area of developing a finite element method for fluid-structure interaction problems, two approaches predominate. The *first approach* is the displacement-based method where the displacements are the nodal variables in both the fluid and the structure. Bathe and Hahn [14], Belytschko [15], Belytschko and Kennedy ([16], [17]), Chopra et al [25] and Nitikitpaiboon and Bathe [53] described the method in detail. This approach is not well suited for problems with large fluid displacements. Another difficulty with this method is that special care must be taken to prevent zero-energy rotational modes from arising. In the

*second approach*, the potential-based method, displacements remain the nodal variables in the structure, while velocity potentials or pressures are the unknowns in the fluid. Everstine [29], Everstine et al. ([30], [31]), Hamdi et al. [34], Morand and Ohayon [51], Ohayon and Valid [56], Olson and Bathe ([58], [59]) and Zienkiewicz et al. ([81], [82], [83]) demonstrated techniques for formulating finite elements using potential-based methods. In all these works, only a linearized version of the problem has been considered.

Several finite element studies have considered gravity and free surface effects along with the fluid-structure interaction. Wilson and Khalvati [75] incorporated the gravity and the free surface effects in a displacement-based method with rotational constraints. Results were demonstrated for both a static and dynamic floating body problem. Their method necessitates the use of a reduced integration scheme to prevent element locking. Aslam [7] incorporated the linearized dynamic free surface condition into a velocity potential-based finite element fluid formulation, but did not consider the fluid-structure interaction problem.

Since variational principles are employed to derive numerical solutions, many researchers have attempted to derive variational functionals for different classes of fluid-structure interaction problems. Abboud and Pinsky [1] (and Pinsky and Abboud [65]) proposed a mixed variational principle for transient and harmonic analysis of non-conservative coupled structure-exterior fluid systems. The formulation provided a

basis for finite element approximation. Kock and Olson [41] presented a finite element formulation directly derived from a variational indicator based on Hamilton's principle. Liu and Uras [45] derived a general variational principle that is not based on *Hamilton's principle*, for fluid-structure interaction problems and demonstrated that several of the fluid-structure interaction formulations, already in use, can be obtained from it. The search for variational principles, resembling Hamilton's principle for fluid mechanics problems, has concerned many researchers including Luke [46], Miles [50], Seliger and Whitham [67], and Serrin [68]. In addition to the variational principles, energy methods have been employed to investigate the problem. Zeng et al. [79] developed an energy-based symmetric coupled finite element/ boundary integral method which is valid for all frequencies.

The various aspects of the kinematic nonlinear interaction of coupled (RC)/soil system under static and dynamic loads are investigated by Shawky and Maekawa [69] through parametric studies of two types of underground structures (Tunnels) subjected to high shear deformations transferred through the nonlinear surrounding soil. Their results show that the minimum thickness of the structure can be computed based on the earth pressure, which is taken as constant and independent of the structural stiffness. The reinforcement ratio and the stiffness of the surrounding soil mainly control the damage level and crack conditions.

Yang [77] uses the finite element method for simulating the response of buried shelters to blast loading due to conventional weapon detonation; taking into account the effects of the soil damping, the stiffness and dimensions of the structure, the source of the weapon detonation and the stand-off distance on shock response. Viscoelasticity is chosen to model the behaviour of the soil material. It is found that rigid structures experience higher pressure and less displacement when compared with more flexible counterparts.

Wolf and Darbre [76] modified both of the weighted-residual technique and the indirect boundary-element method that are well established in the frequency domain. The analysis, then, is to be used in the time domain for nonlinear soil-structure interactions such as a foundation embedded in a layered halfspace when subjected to a vertical earthquake excitation. The new formulation requires a reduced computational effort but in all cases, convolution integrals occur in comparison to the solution in the frequency domain.

Borm [20] investigated the interaction of a massive structure with the ground by solving the equation of wave propagation directly using an explicit method. Three factors influencing the seismic response of a soil-structure system are studied: nonlinear stress-strain soil behavior, energy absorbing side boundaries and special variations of the input motion on the lower boundary. It is concluded that transmitting side boundaries can reduce the maximum response by a high percentage depending on the geometry of the physical model.

Chu et al. [26] proposed an approximate method for the scattering of horizontal shear SH-waves in soil-structure interaction problems by using integral representation of the wave equation. Their results show that foundation

displacements are dependent on the angle of incidence for the cases with elliptical and rectangular foundations.

Often, an analysis of structures and foundations subjected to dynamic loads is performed by assuming perfect bonding at the interfaces at all stages of loading. However, the response of the system can be influenced significantly by the characteristics of the interfaces. Zaman et al. [78] developed a thin layer element for simulation of various modes of deformation in dynamic soil-structure interaction. Four basic modes of deformation are considered: *stick* or *no slip*, *slip* or *sliding*, *separation* or *debonding* and *rebonding*. On the other hand, Leger and Katsouli [43] developed what is called 'gap-friction-elements' having nonlinear constitutive relations to model possible vertical separation and sliding of the foundation-dam interface. It is concluded that the nonlinear interface behavior generally reduces the seismic response of dam-foundation systems and may increase the safety against seismic instability by reducing the base shear to be transmitted to the foundation.

## SOIL-PORE FLUID-STRUCTURE INTERACTION

Soils are multiphase materials exhibiting a strong mechanical coupling between the solid skeleton and the fluid phase. This coupling can be particularly strong in the case of saturated soils of low permeability or under fast transient or dynamic loading, wherein pore pressure plays a significant role. The first successful attempt to develop a model for solid skeleton-pore-fluid interaction is due to Biot [18, 19] for linear elastic materials. This work is followed by further development at Swansea University, where Zienkiewicz and his coworkers ([84], [85], [87], [88], [89], [90]) extended the theory to nonlinear materials and large deformation problems.

Pastor and Merodo [62] proposed a simple mixed finite element formulation in the frequency domain based on displacements and pore pressures as main variables. This can be considered as a fast and valuable tool to provide a first approximation before a full nonlinear analysis in the time domain is performed. The formulation is limited to linear models, with incompressible pore-fluid and very small permeability (i.e., modelling of phenomena such as liquefaction, cyclic mobility or cavitation occurrence are excluded). The results for quay wall analysis under dynamic loading show that incompressibility of pore-fluid may result in volumetric locking of the mesh with a severe loss of accuracy.

Nogami and Kazama [54] developed a three-dimensional thin-layer element for dynamic soil-structure interaction analysis of axisymmetric structures in submerged soil. The formulation is based on Biot's wave equation for fluid-filled porous medium. The results show that the submerged condition affects the characteristics of the Rayleigh waves in soil, alters substantially the soil-structure interaction stresses if the permeability of the soil is relatively large and, to less extent, the response of the structure.

Spyrakos and Xu [72] developed a procedure that can be used for preliminary seismic analysis of intake-outlet towers including soil-structure-fluid interaction. The formulation

considers the effect of partial soil-foundation separation, and the hydrodynamic pressure of the water is accounted for through added masses given in concise closed-form expressions for easy use in analysis and design. Parametric studies are conducted in the presence and absence of surrounding and contained water for typical cases of soil conditions and tower height-foundation width ratios. The results show that hydrodynamic effects are significant and cause an increase in deflections, moments and shears and a decrease in foundation rotation. The study also shows that for short towers, foundation uplift is unlikely to occur. Whereas, for slender towers, uplift is more likely to appear, especially for foundations supported by stiff soil, causing significant decrease in moments and deflections.

Guan and Moore [33] proposed a frequency domain procedure for dynamic analysis of reservoir-dam systems resting on a multi-layered soil when subjected to El-Centro earthquake ground motion (1940). The confined fluid is assumed viscous to account for the internal viscosity and absorption at the reservoir bottom. The dam was modelled using the finite element method and the stiffness matrix of the layered soil is obtained by means of the layer transfer matrix. The procedure also avoids any additional discretization of the fluid and the foundation except at their interfaces with the dam structure.

Zienkiewicz [80] described extensively several kinds of coupled problems and their numerical solution with some applications. The analysis of coupled soil-pore- fluid interaction during an earthquake shock applied to a dam shows that the non-linear soil response causes a pore pressure build up and failure of the actual structure.

Park and Felippa [61] reviewed several developments of computational procedures for solving coupled field problems with emphasis on stabilization of partitioned analysis. It is found that the resulting matrices after semi-discretization are not symmetric. The non-symmetry in the matrices often induces *conditional stability* of partitioned solutions and, therefore, stabilization is necessary at the differential equation level before attempting to implement a partitioned solution procedure.

Barbat [9] studied the seismic response of elevated water tanks using the substructure approach, taking into account the effect of the overturning moment, which affects the general stability of the structure, the effect of water's vibration in the tank and the effect of bending moment in the tower-foundation cross-section. The tank is idealized by shell elements while the soil and the water are treated by isoparametric solid finite elements. The horizontal component of the Taft, 1952, earthquake is used as an input. The results show 21% increase on the acceleration response due to the fluid-structure interaction plus an additional 15% increase when the foundation ground effect is also taken into consideration.

The behavior of multiphase flow in deforming porous media is of interest in engineering problems such as the simultaneous flow of three immiscible fluids; e.g. gas, oil and water through tar sand formation during the bitumen recovery process, with environmental studies, etc. For most cases of fluid transport in soil, two or more fluid phases are presented

simultaneously in the pores and are separated from one another by interfaces.

Li and Zienkiewicz [44] developed a numerical procedure for modelling the behaviour of porous media interacting with the flow of multiphase immiscible fluids based on Biot's theory and the principle of effective stress. The displacement of the solid, pressure and saturation of the wetting fluid are taken as primary unknowns of the model. Unconditionally stable direct and staggered solution procedures are used in the time domain while the numerical solution of the coupled finite element equations are set with  $u-p_w-S_w$  form and discretized by Galerkin's method.

Naylor [52] investigated the stress accuracy at a very low compressibility through the calculation of excess pore pressures by means of finite element analysis of porous media. It is found that the mean stress becomes grossly in error at the center and edges of each element as the compressibility are reduced whereas, the deviator stress components do not.

## CONSTITUTIVE RELATIONS OF SOIL

### Isotropic Hardening Cap Models

The cap plasticity model has been used widely in recent years in finite element analysis programs for a number of geotechnical engineering applications, Chen and McCarron [23] and McCarron and Chen [49].

Various types of cap models have been developed at Cambridge University (Cam-clay and Modified Cam-clay models) using a cap as part of the yield surface with critical state soil plasticity. DiMaggio and Sandler [27] developed a generalized cap model for rocks by allowing only expansion of the cap (i.e. hardening). Due to that, the cap is not reversible; therefore, it allows representation of a relatively large amount of dilatancy that occurred during failure of rocks at low pressures. Anisotropy may also be achieved by introducing pseudo-stress-invariants, which are similar in form to stress-invariants but include weighting factors on the stress components in different directions. These modified cap models are now widely used in ground shock computations in soil mechanics problems.

### Constitutive Models for Sands

The irreversible behavior of sands has been simulated with various types of constitutive models. Among the models, the bounding surface plasticity one is found capable of providing a flexible theoretical framework to model the significant features of loose and dense sands behavior under not only cyclic but also monotonic loading and is simple enough to be used in practical applications, e.g. (Aboim and Roth [3]), (Bardet [10], [11]) and (Hashigushi and Ueno [35]).

Oka and Washizu [57] proposed a constitutive model that can describe the cyclic behaviour of sands based on elasto-

plasticity and the concept of the boundary surface. The ‘relative stress ratio’ and the newly defined parameter ‘relative deviatoric strain’ are used to formulate the hardening function. The model can be used for liquefaction analysis, as it can explain the behaviour of sands after the stress ratio attains the value defined by the phase transformation angle.

Using bounding surface plasticity, Bardet ([12], [13]) developed a constitutive model for simulating the nonlinear behaviour of loose and dense sands subjected to various types of loadings. The critical state, which depends upon the initial void ratio, defines the evolution of the bounding surface during plastic flow. Bardet’s model describes strain softening and stress-dilatancy with nine material constants calculated from the results of conventional triaxial tests. It is also capable of simulating drained and undrained responses, hysteric energy dissipation and accumulation of irreversible strains during cyclic laboratory tests and liquefaction analysis.

A constitutive model for sand, within the general framework of bounding surface hypoplasticity, is formulated by Wang et al. [74]. The distinction of the model is the dependence of the loading and plastic strain rate directions on the stress rate direction. This property being the reason behind the successful simulation of the response under “rotational shear” that related to the liquefaction phenomenon, which may occur under such cyclic loading conditions of a complex nature.

The capabilities of the bounding surface plasticity model of Bardet ([12], [13]) have been validated using two boundary value problems by Altaee et al. [6]. In the first boundary value problem, the finite element program, which incorporates the bounding surface model, is used to simulate the load-displacement behavior of a model-scale footing. In the second analysis, the behavior of Leighton Buzzard Sand in Cambridge simple shear device is predicted and the results are compared with the measurements. In both validation problems, a good agreement is obtained between the measured and calculated results.

Zienkiewicz et al. [90] developed a simple model of a generalized plasticity-bounding surface type for describing sand response under cyclic loading. The model is also capable of predicting the ‘liquefaction potential’ and improves the performance of critical state models in monotonic loading (by addition of a single parameter to those required for a standard, critical state model). However, the new model is still incapable of reproducing adequately the phenomena of complete liquefaction and cyclic mobility observed in sands.

Pastor et al. [63] extended their first bounding surface plasticity model to simulate the behaviour of sands under both static and transient loadings. The essential features of the first model are preserved but with the following changes are introduced separately: (i) Modifying the shape of the yield surface, (ii) Introducing a non-associative flow rule, (iii) Including of deviatoric plastic strains in the hardening parameter of the bounding surface and (iv) Introducing a plastic volumetric and deviatoric strains during unloading. In the new model, the direction tensors of plastic flow and the

corresponding plastic moduli are interpolated from a ‘critical state’ plasticity form of a bounding yield surface of elliptic shape.

## MATERIAL MODELS OF REINFORCED CONCRETE

### Concrete in Compression

The following conditions have to be considered in establishing the nonlinear stress-strain relations based on the theory of plasticity (Hill [36]):

(a) The yield criterion: The strength of concrete under multidimensional states of stress is a function of the state of stress itself and can not be predicted by limitations of simple tensile, compressive and shearing stresses independently of each other. Therefore, a proper evaluation of concrete strength can be achieved by considering interaction of the various components of the state of stress. Many yield criteria have been developed to describe the strength of concrete (Chen [22]). The one adopted herein is the Drucker Prager Model.

### Biaxial Stress Envelopes

The failure criterion under biaxial loading proposed by Kupfer and Gerstle [42] is shown in Fig. (1). This criterion has been adopted as a failure criterion by some authors. The yield criterion adopted here is of such a type as that used by Thannon [73] and Shukr [70].

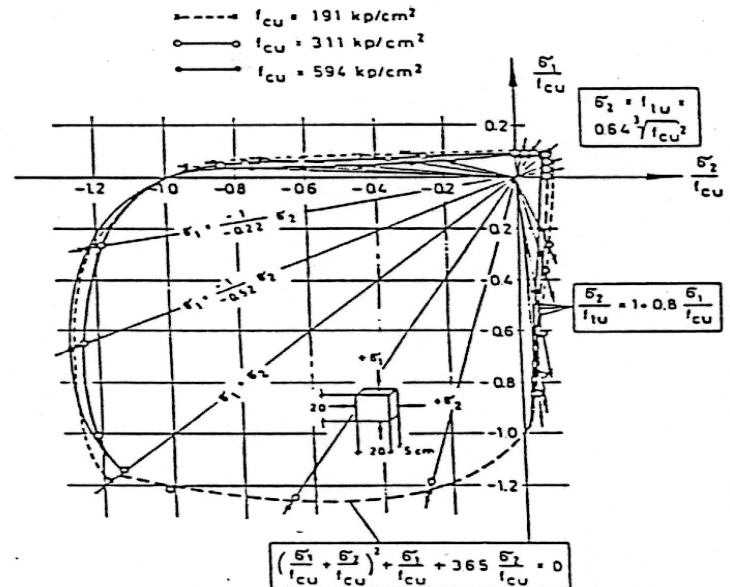


Fig. (1): Biaxial strength envelopes (Kupfer and Gerstle, [42]).

(b) The flow rule: To construct the stress-strain relationship in the plastic range, an *associated flow rule* will be employed.

This means that the plastic deformation rate vector will be assumed to be normal to the yield surface.

(c) The hardening rule: The hardening rule is necessary to define the evolution of positions of the “loading surface” during plastic deformation. A relationship between the accumulated plastic strain and the effective stress is required to control the position of the current “loading surface”. In the present work, the relation between effective stress and effective plastic strain is extrapolated from the uniaxial stress-strain relationship using the conventional “*Madrid Parabola*” as in Ref. [47].

(d) The crushing condition: The crushing type of concrete fracture is a strain-controlled phenomenon. A failure surface in the strain space must be defined so that this kind of fracture can be taken into account. This feature is incorporated into the model by converting the yield criterion (described in terms of stresses) directly into strain (Hinton [37]).

### Reinforcement Representation

The mechanical properties of steel are, in comparison to concrete, well known and understood. Steel is homogeneous and has usually the same yield strength in tension and compression. In the present study, a bilinear stress-strain relationship allowing for strain hardening and elastic-perfect plastic relation is used.

### Concrete in Tension

In this study, concrete in tension is modelled as a linear-elastic brittle material (Abdul-Aziz [2]) and the maximum tensile stress criterion (tension cut-off) is employed. In the present study, the smeared crack representation is adopted for crack modeling, implying that the cracks are distributed across a region of the finite element. Before cracking, concrete is initially considered to be as an isotropic material.

## DEFINITION OF COUPLED PROBLEMS

Coupled systems and formulations are those applicable to multiple fields and dependent variables, which usually (but not always) describe different physical phenomena, and in which:

- (i) neither field can be solved accurately while separated from the other, and
- (ii) neither set of dependent variables can be explicitly eliminated without inversion at the differential equation level.

### Types of Coupled Systems

Coupled systems can be classified into two classes:

Class I: This class contains problems in which coupling occurs on field interfaces via the boundary conditions or between

fields that are physically similar in which different discretization processes have been used. Some examples of this type of coupling are shown in Fig. (2). The need for the use of different discretizations may arise from different causes (Zienkiewicz and Taylor [86]):

- (1) different finite element meshes may be advantageous to describe the subdomains.
- (2) different procedures such as the combination of boundary method and finite element in respective regions may be computationally desirable.
- (3) domains may simply be divided by the choice of different time stepping procedures, such as implicit and explicit algorithms.

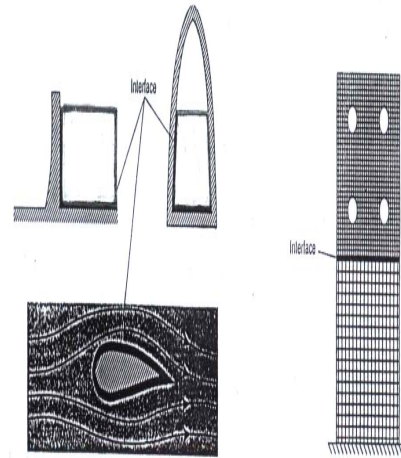


Fig. (2): Class I coupled problems with coupling via interfaces (shown as thick lines).

Class II: This class contains problems in which the various fields overlap (totally or partially). Here the coupling occurs through the differential governing equations describing different physical phenomena.

### Fluid-Structure Interaction (Class I Coupling)

The general topic of dynamic fluid-structure interaction needs all the aspects associated with both structural dynamics and fluid dynamics. Each of these two areas is complex by itself; moreover, when considered together, the situation becomes more complicated. In fact, the coupling between fluid and solid responses can be viewed as a feedback loop of the type shown in Fig. (3). The structure surface loading is not known a priori but depends on the interface pressures in the fluid and the fluid response is, in turn, a function of the structure’s surface motion (Donea [28]).

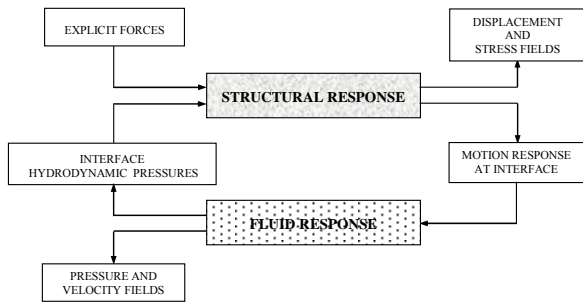
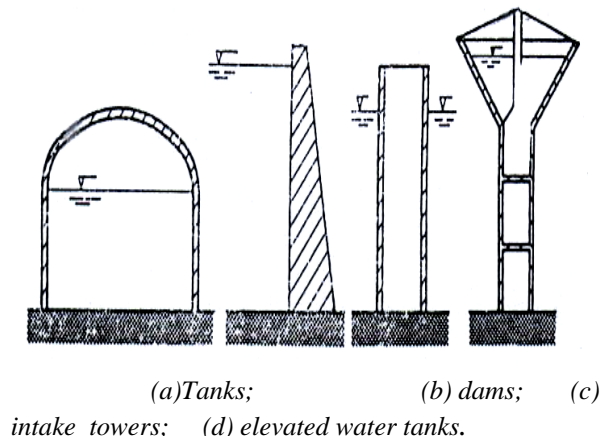


Fig. (3): Feedback loop in fluid-structure problems (Donea [28]).

The finite element method (FEM) can be employed as a numerical tool to solve coupled fluid-structure problems under dynamic loadings with three distinct tasks involved: (1) the development of a fluid analysis algorithm, (2) the development of a structural analysis algorithm and (3) coupling the fluid and structure algorithms.

The formulation of the seismic analysis problem of a structure, when it includes the fluid-structure interaction, is greatly influenced by the fluid-substructure boundary shape. In most cases, the interaction problem is defined as a class I; coupling through the boundary conditions. The most important cases in which a construction must be analyzed under fluid-structure coupling conditions may be classified into:

- The fluid is contained within the structure, such as in the case of tanks (Figure 4a and 4d).
- The fluid is stored only at one side of the structure, such as in the case of dams (Figure 4b).
- The structure is partially or totally submerged in fluid, such as in the case of intake towers (Figure 4c) and offshore gravity platforms.



(a) Tanks; (b) dams; (c) intake towers; (d) elevated water tanks.

Fig. (4) Fluid-structure interaction

To obtain a general formulation, valid for all the above cases, the problem of fluid-structure interaction can be solved by the substructuring method as shown in (Fig. 5). The solution may be established by means of an analysis in the time domain or transforming the equations of motion to the complex frequency

domain, using either the Fourier or Laplace Transform actions. But, the difficulties involved in the formulation are: (i) the numerical definition of the additional masses which simulate the fluids' vibrations and (ii) the numerical definition of the damping and the stiffness characteristics of the model (Chopra and Chakrabarti [24]).

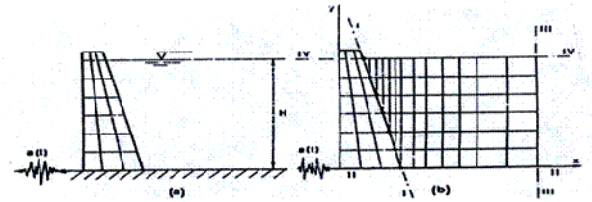


Fig. (5): Fluid-structure interaction: generic formulation of the problem.

- (a) Structure discretized by finite elements, in contact with a fluid medium,
- (b) Substructure analysis model.

### Soil-Pore-Fluid Interaction (Class II Coupling)

This class contains problems in which the various fields overlap (totally or partially) (Fig. 6).

Pore fluid-solid interaction is important in materials like saturated sand, clay and rock under dynamic conditions. These materials when saturated with fluid can be treated as two-phase materials, as in earth dams, sand drains, etc.....

As the total stress present in the soil can be divided into two parts; the effective stress and the pore pressure, deformations or strains of the solid skeleton arise only if there is a change in the effective stress. In certain cases, the pore pressure may reach a value equal to the total stress and lead to

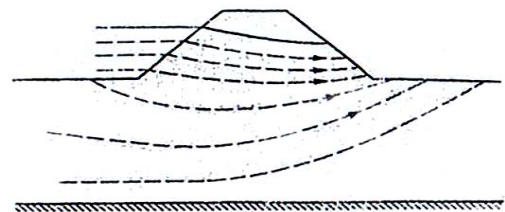


Fig. (6): Class II coupled problems with overlapping coupling.

zero effective stress and if the soil is sand it may liquefy (i.e., flows like a liquid because of the loss of its shear strength).

If the permeability of the soil medium is high, then, there will be some dissipation of excess pore pressure. This case duplicates the drained condition, in which the pore pressure remains, unchanged.

But, under earthquake loading, the exciting force is applied so suddenly (short term loading) that no flow of pore fluid can take place in the interstitial pores of the saturated soil. Consequently, a complete undrained condition applies and the two phases deform and produce a common strain in both solid and fluid phases. In other words, the change in effective stress

and the change in excess pore water pressure can, therefore, both be related to the same common change in strain if the soil is assumed to be fully saturated. This change in excess pore water pressure results in a change of volumetric strain in the soil skeleton (Chang et al. [21]).

**BLAST LOADING**

Only limited information are available as a database; almost all dynamic laboratory testing techniques use sinusoidal loading as a type of force excitation. In field testing, seismic waves are generated by either an impact force or by detonation of small charges (Aggour et al. [4]). Therefore, much of the information are highly empirical and can be assembled from the military, which belong to occurred incidents and simple testing.

The blast wave generated in an explosion, imposes a dynamic load on any object in its field. This dynamic load is characterized by rapidly reaching a peak value within a very short period of time, then after that decreases as the blast wave decays. The first mechanical effect of an explosive blast is a forceful blow from the instantaneous pressure jump in its shock front. This is followed immediately by the crushing effect of blast overpressure (pressure above atmospheric) and a blast wind of high velocity. Representative effects are indicated in (Fig. 7) along with the pressure variation of typical blast wave (Kinney and Graham, [40]). Times A to D, indicated in this figure, correspond to those shown in the pressure variation diagram. At time A, the atmosphere is still undisturbed. Time B is immediately after the shock wave has reached the structure. At time C, there is a slight negative phase along with a reversed blast wind.

With the propagation of blast wave, the shock front pressure will decrease (the wave expands) and the wave duration will increase. Therefore, a variation in the magnitude of blast loads with the increased distance from the explosion source is expected. In general, the total blast effect on any structure may be assumed to consist of the following three main components: (i) the initial reflected pressure, (ii) the incident overpressure and (iii) the drag pressure (blast wind).

The net effect of blast loading is determined by the interaction of the above three parts, which would depend on the geometry of the structure and its position relative to the explosive source. In order to analyze any structure subjected to blast loading, a suitable simulation of these loads is necessary.

High Explosive Bombs

An explosion is the result of a very rapid release of large amounts of energy within a limited space and in a very short time. When an explosion is taking place, the explosion of the hot gases produces a pressure wave in the surrounding air due to a sudden increase in the volume of produced gases due to chemical reactions that involve a rearrangement of the atoms in the case of conventional (non- nuclear) explosions.

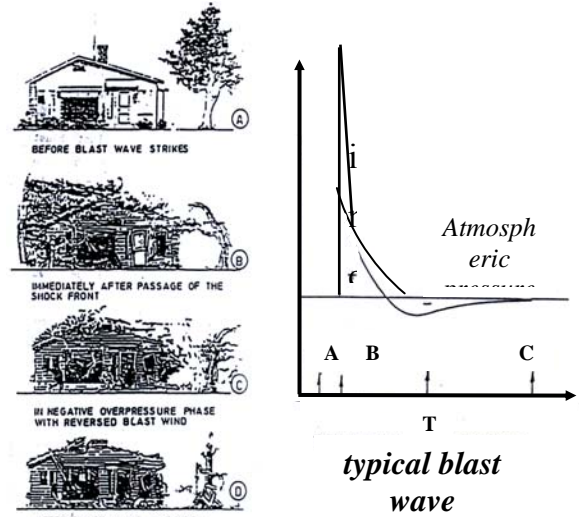


Fig. (7): Pictorial representation of blast wave effects for different time of wave propagation, (Ayvazyan et al., [8]).

As the wave moves away from the center of explosion, the inner part moves through the region that was previously compressed and is now heated by the leading part of the wave. As the pressure wave moves with the velocity of sound, the temperature and pressure of the air cause this velocity to increase. The inner part of the wave starts to move faster, and gradually overtakes the leading part of the wave. After a short period of time, the pressure wave front becomes abrupt, thus forming a shock front somewhat similar to the one illustrated in Fig. (8a). In near-zones, detonation products and shocked air interact to give a composite blast effect, whereas, in far-zones only the atmosphere is involved. Consequently, the over-pressure is given according to (Norris et al. [201]):

$$P / P_{\max} = (1 - t/t^+) \cdot \exp(-c \cdot t/t^+) \dots\dots\dots(1)$$

where:  $t$  = the time after passing of the shock,  $t^+$  = the duration of the positive pulse, and  $c$  is a constant that represents the wave form parameter which measures the rate of decay of the pressure. This expression is valid only for the positive phase and the portion of the negative phase equal to  $(1.5-1.8) t^+$ . The relation between the blast impulse and the decay parameter is obtained by integrating Equation (1).

$$\frac{I}{A} = \frac{\text{impulse}}{\text{unit area}} = \int_0^{t^+} P dt = P_{\max} t^+ \left[ \frac{1}{c} - \frac{(1 - \exp^{-c})}{c^2} \right] \dots\dots\dots(2)$$

Equation (2) provides values for the blast wave impulse per unit area when the wave form parameter  $c$  is known. Inversely, knowing the blast impulse per unit area, the wave

form parameter may be obtained from Equation (1).

The maximum overpressure occurs at the shock and is called the peak overpressure ( $P_{max}$ ) whereas behind the shock front, the overpressure drops very rapidly to about one-half the peak value and remains almost uniform in the central region of the explosion (Figure 8b). As the expansion precedes, the overpressure in the shock front decreases steadily; while the pressure behind the front does not remain constant but instead, falls off in a regular manner. After a short time, at a certain distance from the center of the explosion, the pressure behind the shock front becomes smaller than of the surrounding atmosphere and the so-called negative phase, or suction develops. The front of the blast wave weakens as it progresses outward and its velocity drops to the velocity of sound in the undisturbed atmosphere. This sequence of events, at successive times is shown in (Figure 8c).

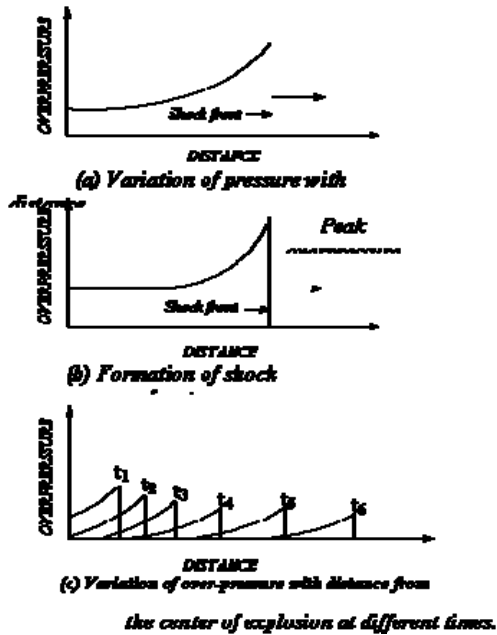


Fig. (8): Shock wave pressure-time variation (Fertis, [32]).

Johnson [38] has published an equation for maximum pressure  $P_{max}$ , which after modification to SI units is:

$$P_{max}, s = (455/z^3) - (4.60/z^2) + (0.70/z) \dots\dots\dots(3)$$

where:  $P_{max}$  is in (MPa) ,  $z = r/w^{1/3}$ ,  $r$  = distance from charge  $w$  in meters,  $w$  = charge in (kg). The peak pressure  $P_{max}$  determines the damage level, which can be divided into:

- (i) Primary: occurring due to the direct effect of the blast and the pushing-over of part of the structure.
- (ii) Secondary: occurring due to the subsequent collapse of other parts.

**GOVERNING EQUATIONS FOR THE DYNAMIC PROBLEMS AND COUPLED FORMULATIONS**

The dynamic analysis of soil-fluid-structure interaction includes all aspects of both fluid and solid mechanics (i.e., fluid-structure interaction (class I coupling) and soil-pore-fluid

interaction (class II coupling)). In a fluid-phase, the viscosity of the fluid, the magnitude of the gradient of the velocity field throughout the flow and whether the fluid is (compressible or incompressible), depending on whether density variations are large or small, play a key role in choosing the kind of formulation to be used. Whereas in the solid-phase, the time scale and the solver algorithm to be used depends on the loading rate and the permeability of the porous medium.

Fluid-Structure Interaction (Class I Coupling)

The Governing Equations of Fluid Dynamics

(a) Governing Equation of Motion

The following well-known wave Equation (Joseph [39]) is started with:

$$\nabla^2 P + \xi' \nabla^2 \dot{P} = \ddot{P}/c^2 \quad \text{Linearized-Navier-Stokes Equation).....(4)}$$

where:  $\xi' = 4\mu'/3\rho_f c^2$ ,  $\mu'$  = the dynamic viscosity of fluid and  $c^2 = K/\rho$ .

For an inviscid fluid, Equation (4.13) reduces to:

$$\nabla^2 P = \ddot{P}/c^2 \dots\dots\dots(5)$$

(b) Boundary Conditions:

- (i) At moving boundaries (at interface with solid) where the fluid has a normal acceleration,  $\ddot{u}_n$ ,  $n$  being the direction of the unit normal to the boundary, the pressure gradient can be expressed as:

$$\partial P/\partial n = -\rho_f \ddot{u}_n \dots\dots\dots(6)$$

At fixed boundaries;  $\partial P/\partial n = 0$ .

- (ii) At a free surface with surface waves (considering only primary waves):

$$P = \rho_f g u_y \quad \text{or} \quad \partial P/\partial y = \ddot{p}/g \dots\dots\dots(7)$$

At a free surface without surface waves:  $P = 0$ .

- (iii) At radiating boundaries, the condition for no reflection of pressure waves can be expressed as:

$$\partial P/\partial n = -\dot{P}/c \dots\dots\dots(8)$$

where:  $n$  = the direction of the unit normal at the radiating boundary.

Fluid Isoparametric Element

The fluid domain is usually represented by finite elements in Cartesian coordinates. The number of nodes may be variable (4-9) in two dimensions, with one degree of freedom

per node inside the fluid domain. This degree of freedom is the value of the pressure P at the nodes. At the free surface, the element has an extra translational degree of freedom to accommodate the free surface motion. This element enforces the continuity (equilibrium in solids) equation along the mesh domain. The applied forces represent the water pressure at the nodes. The positive pressure is in-pressure and the negative one is out-pressure. For global equilibrium, the in-pressure must be equal to the out-pressure. At the boundaries, only the normal force may be specified because the tangential force does not affect the pressure. The nodal equilibrium is satisfied if the sum of the water pressure increments at the node is equal to the total applied pressure.

### Fluid-Solid Contact Node

This node causes the fluid-structure interaction matrix to be generated and assembled to the left-hand side. Also, it transforms the structure normal force to a pressure vector, applies it on the fluid nodes, transforms the fluid pressure to a force vector and applies it on the structure nodes in the normal direction.

### Soil-Pore Fluid Interaction (Class II Coupling)

This formulation represents a more general one that best simulates the behaviour of granular soils under dynamic loading and especially blast loading due to the large voids of such materials. This is attributed to the shape, size and rearrangement of soil particles, which allow easy movement of the pore fluid, and this, in turn, increases the fluid inertia. The model assumes p as the nodal pore-fluid pressure in the finite element discretization and both the solid grains and fluids to be compressible, taking into account the fluid inertia effects. Zienkiewicz and Bettess [82] verified this model when high frequency loads are applied.

### The u-p Formulation (medium-speed phenomenon)

When the changes in relative velocity  $\dot{W}$  are assumed to be small, or if the permeability is low, the variable  $w_i$  is usually eliminated so that  $\ddot{W}$ ,  $\rho \ddot{W}$  and  $(\rho/n) w$  can be neglected with the assumption that  $\ddot{W}_i / \ddot{u}_i \rightarrow 0$ . With this approximation, the unknown quantity  $w_i$  can be replaced by the pressure P, retaining only  $u_i$  and P as the basic variables. According to this assumption, the set of equations governing the problem can be written as follows (Zienkiewicz and Bettess [82]):

$$d\varepsilon_{ij} = (du_{i,j} + du_{j,i}) / 2 \dots \dots \dots (9)$$

$$\sigma_{ij} = \sigma'_{ij} + \delta_{ij}P \dots \dots \dots (10)$$

$$d\sigma'_{ij} = D_{ijkl} (d\varepsilon_{kl} - d\varepsilon^0_{kl} + \delta_{kl} dP / 3K_s) \dots \dots \dots (11)$$

$$\sigma_{ij,j} + \rho_t g_i = \rho_t \ddot{u}_i \dots \dots \dots (12)$$

$$\begin{aligned} (k_{ij}P_{,j})_{,i} - \dot{\varepsilon}_{ii} - (k_{ij} \rho_f g_j)_{,i} &= n \dot{P} / K_f + (1-n) \dot{P} / K_s - \dot{\sigma}'_{ii} / 3K_s \\ &- (k_{ij} \rho \ddot{u}_j)_{,i} \dots \dots \dots (13) \end{aligned}$$

The first four equations represent simple dynamic behaviour and the fifth is an augmented form of the transient seepage equation. In matrix form:

$$\begin{bmatrix} M_s & 0 \\ -\hat{M} & 0 \end{bmatrix} \ddot{u} + \begin{bmatrix} C_s & 0 \\ L^T & C_p \end{bmatrix} \dot{u} + \begin{bmatrix} K_s & -L \\ 0 & K_p \end{bmatrix} u = \begin{bmatrix} f_s \\ f_p \end{bmatrix} \dots \dots \dots (14)$$

One advantage of this approximation is the reduction in size of the equation set. However, the coefficient matrices in the coupled discretized equilibrium equation are non-symmetric and involve the solution of unsymmetric equations with large number of variables. Therefore, the staggered solution process based on a predictor-corrector iteration scheme overcomes those difficulties (Simon et al. [71]). In the present study, this formulation is implemented with the staggered solution for the time integration algorithm in the developed algorithm.

## DISCRETIZATION BY THE FINITE ELEMENT METHOD

### Fluid-Structure Interaction (Class I Coupling)

#### Assumptions

In the fluid-solid models, the following assumptions are made:

- (i) the fluid is linear, compressible and inviscid.
- (ii) the flow is considered irrotational.
- (iii) there is no friction between the fluid and solid (no boundary layer).
- (vi) thermal effects are negligible.
- (vii) the solid may undergo plastic deformations.

### The u-p Formulation

The structure and fluid are together idealized as a two dimensional system subjected to support excitation both in the horizontal and vertical directions. The equations of motion can be expressed, after spatial discretization, by two sets of second order coupled differential equations. The fluid can be modeled using any of the various formulations (pressure, displacement, velocity potential and displacement potential). However, in this study only the pressure formulation is used in which the coupled fluid-structure equations can be expressed as (Al-Nu'aimy [10]):

$$M_s \ddot{u} + C_s \dot{u} + K_s u = f_s - M_s \ddot{d} + L P \dots \dots \dots (15)$$

$$M_f \ddot{P} + C_f \dot{P} + K_f P = f_f - \rho_f L^T (\ddot{u} + \ddot{d}) \dots \dots \dots (16)$$

where:

$$\underline{M}_s = \int_{\Omega} \underline{N}_u^T \rho \underline{N}_u d\Omega \quad (17)$$

$$\underline{C}_s = \alpha \underline{M}_s + \beta \underline{K}_s \quad \text{(Rayleigh Damping)} \quad (18)$$

$$\underline{K}_s = \int_{\Omega} \underline{B}^T \underline{D}_T \underline{B} d\Omega \quad (19)$$

$$\underline{f}_s = \int_{\Gamma_u} \underline{N}_u^T \underline{t} d\Gamma + \int_{\Omega} \underline{N}_u^T \rho \underline{b} d\Omega + \int_{\Omega} \underline{B}^T \underline{D}^T d\varepsilon^o d\Omega \quad (20)$$

$$\underline{L} = \int_{\Omega} \alpha_c \underline{B}^T \delta \underline{N}_p d\Omega \quad (21)$$

$$(\underline{M}_f)_{ij} = \int_{\Gamma_F} \underline{N}_{pi} 1/g \underline{N}_{pj} d\Gamma + \int_{\Omega_F} \underline{N}_{pi}^T 1/c^2 \underline{N}_{pj} d\Omega \quad (22)$$

$$(\underline{C}_f)_{ij} = \int_{\Gamma_R} \underline{N}_{pi}^T 1/c^2 \underline{N}_{pj} d\Gamma \quad (23)$$

$$(\underline{K}_f)_{ij} = \int_{\Omega_F} (\nabla \underline{N}_{pi})^T (\nabla \underline{N}_{pj}) d\Omega \quad (24)$$

$$(\underline{L}^T)_{ij} = \int_{\Gamma_I} \underline{N}_{ui}^T n \underline{N}_{pj} d\Gamma \quad (25)$$

### Special Cases for Class I Coupling

#### (i) Rigid Structure and Incompressible Fluid

The assumption of a rigid structure implies that Equation (15) vanishes and that Equation (16) reduces to:

$$\underline{K}_f \underline{P} = -\rho_f \underline{L}^T \ddot{\underline{d}} \quad (26)$$

#### (ii) Rigid Structure and Compressible Fluid

Again consideration of a rigid structure implies that Equation (5.1) vanishes and Equation (5.2) reduces to:

$$\underline{M}_f \ddot{\underline{P}} + \underline{C}_f \dot{\underline{P}} + \underline{K}_f \underline{P} = -\rho_f \underline{L}^T \ddot{\underline{d}} \quad (27)$$

#### (iii) Flexible Structure and Incompressible Fluid

For an incompressible fluid, the speed of sound  $c$  in the fluid is taken to be infinity. The matrices  $\underline{M}_f$  and  $\underline{C}_f$  in Equation (16), therefore, vanish and the Equations reduce to:

$$\underline{M}_s \ddot{\underline{u}} + \underline{C}_s \dot{\underline{u}} + \underline{K}_s \underline{u} = \underline{f}_s - \underline{M}_s \ddot{\underline{d}} + \underline{L} \underline{P} \quad (28)$$

$$\underline{K}_f \underline{P} = -\rho_f \underline{L}^T (\ddot{\underline{u}} + \ddot{\underline{d}}) \quad (29)$$

Solving Equation (5.7) for  $\underline{P}$ , gives:

$$\underline{P} = -\rho_f \underline{K}_f^{-1} \underline{L}^T (\ddot{\underline{u}} + \ddot{\underline{d}}) \quad (30)$$

and substituting equation (30) in Equation (28) gives:

$$\underline{M}_{sf} \ddot{\underline{u}} + \underline{C}_s \dot{\underline{u}} + \underline{K}_s \underline{u} = \underline{f}_s - \underline{M}_{sf} \ddot{\underline{d}} \quad (31)$$

where:  $\underline{M}_{sf} = \underline{M}_s + \underline{M}_{ff}$   
 $\underline{M}_{ff} = \rho_f \underline{L} \underline{K}_f^{-1} \underline{L}^T$  (added mass)

The effect of an incompressible fluid on a flexible dam is an additional mass and an additional force, well known as the virtual mass and virtual force. Direct integration of coupled

Equations (28) and (29) by a partitioned solution scheme becomes unstable due to the infinite sound speed in the fluid and the solution fails (Paul [64]). However, the structural response can be evaluated from Equation (31) directly and the pressure can be evaluated from Equation (30).

### Pore Fluid–Solid Interaction (Class II Coupling)

#### The u-p Formulation

When the seepage velocity relative to the solid skeleton is small compared with the motion of the solid skeleton or if the permeability is low, the relative acceleration of the fluid with respect to the solid can be neglected. With this approximation (i.e., neglecting the  $\dot{\underline{w}}$  term) and replacing the unknown  $w$  with the pressure  $P$ , the equilibrium equation of the fluid can be rewritten as (Paul [64]):

$$\dot{\underline{w}} = -k \nabla P + k \rho \underline{b} - k \rho \ddot{\underline{u}} \quad (32)$$

which can be used to eliminate  $w$  from the continuity equation. Upon discretization, it is possible to write:

$$\underline{u} = \underline{N}_u \underline{u} \quad (33)$$

$$\underline{P} = \underline{N}_p P \quad (34)$$

and using the standard Galerkin method, the resulting equations can be expressed as:

$$\underline{M}_s \ddot{\underline{u}} + \underline{C}_s \dot{\underline{u}} + \underline{K}_s \underline{u} = \underline{f}_s - \underline{M}_s \ddot{\underline{d}} + \underline{L} \underline{P} \quad (35)$$

$$\underline{C}_p \dot{\underline{P}} + \underline{K}_p \underline{P} = \underline{f}_p - \underline{L}^T \dot{\underline{u}} + \hat{\underline{M}} \ddot{\underline{u}} \quad (36)$$

where:

$$\underline{M}_s = \int_{\Omega} \underline{N}_u^T \rho \underline{N}_u d\Omega \quad (37)$$

$$\underline{C}_s = \alpha \underline{M}_s + \beta \underline{K}_s \quad \text{(Rayleigh Damping)} \quad (38)$$

$$\underline{K}_s = \int_{\Omega} \underline{B}^T (\underline{D}_T + \alpha_c^2 \delta \cdot Q \cdot \delta^T) \underline{B} d\Omega \quad (39)$$

$$\underline{f}_s = \int_{\Gamma_u} \underline{N}_u^T \underline{t} d\Gamma + \int_{\Omega} \underline{N}_u^T \rho \underline{b} d\Omega + \int_{\Omega} \underline{B}^T \underline{D}^T d\varepsilon^o d\Omega \quad (40)$$

$$\underline{L} = \int_{\Omega} \alpha_c \underline{B}^T \delta \underline{N}_p d\Omega \quad (41)$$

$$\underline{C}_p = \int_{\Omega} \underline{N}_p^T 1/Q \underline{N}_p d\Omega \quad (42)$$

$$\underline{K}_p = \int_{\Omega} (\nabla \underline{N}_p)^T k (\nabla \underline{N}_p) d\Omega \quad (43)$$

$$\underline{f}_p = \int_{\Gamma_p} \underline{N}_p^T P d\Gamma + \int_{\Omega} (\nabla \underline{N}_p)^T k \rho_f \underline{b} d\Omega \quad (44)$$

$$\underline{L}^T = \int_{\Omega} \alpha_c \underline{N}_p^T \delta \underline{B} d\Omega \quad (45)$$

$$\hat{\underline{M}} = \int_{\Omega} (\nabla \underline{N}_p)^T k \rho_f \underline{N}_u d\Omega \quad (46)$$

where:  $\underline{N}_p$  and  $\underline{N}_u$  are the shape functions used for pore pressure and solid skeleton, respectively.  $\alpha$  and  $\beta$  are Rayleigh damping constants,  $\Omega$  = the domain,  $\Gamma$  = the boundary surface,



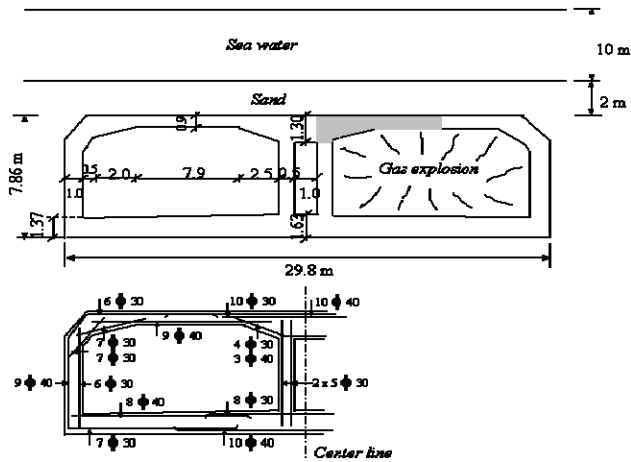


Figure (10): Typical tunnel cross-section with reinforcement for 1.5 m wide section (Mier, [48]).

### Loading cases

Three loading cases are considered: dead weight (gravity load), uniformly distributed vertical load (sand and water) and gas explosion (internal pressure). Figure (11) summarizes the load cases relevant to all the analyses.

For determining the dead weight of the tunnel, the density of the concrete is taken as  $2400 \text{ kg/m}^3$  which corresponds to a density input value of  $2.4 \text{ (kN-sec}^2/\text{m}^4)$  and should be combined with a gravity acceleration of  $9.81 \text{ m/sec}^2$ . For the soil weight, a 2-m layer of sand weighing  $1900 \text{ kg/m}^3$  is assumed and a 10-m depth of water weighing  $1000 \text{ kg/m}^3$  is included. Soil and water exert a pressure of  $0.1353 \text{ kN/m}$  on a 1-m wide of the tunnel.

Table (10.11): Material properties for the problem (Mier, [48]).

Material and Property	Value
<b>1. Concrete</b>	
Young's modulus	$E_c = 22 \times 10^6 \text{ (kPa)}$
Poisson's ratio	$\nu = 0.2$
Ultimate Compressive stress	$f_c = 30 \times 10^3 \text{ (kPa)}$
Ultimate Compressive strain	$\epsilon_{us} = 0.0010$
Crushing strain	$\epsilon_{cu} = 0.0035$
Tensile strength	$f_t = 3.36 \times 10^3 \text{ (kPa)}$
Cracking strain	$\epsilon_{cr} = 0.000075$
Elastic limit	0.3
Mass density	$\rho = 2400 \text{ (kg/m}^3)$
<b>2. Steel</b>	
Young's modulus	$E_s = 21 \times 10^7 \text{ (kPa)}$
Yield stress	$f_y = 528 \times 10^6 \text{ (kPa)}$
<b>3. Soil (sand)</b>	

Young's modulus, E	$26 \times 10^3 \text{ (kPa)}$
Poisson's ratio, $\nu$	0.37
Density, $\rho$	$1900 \text{ (kg/m}^3)$
<b>Cap model parameters:</b>	
A = $0.203 \times 10^{-2} \text{ (kPa)}$	B = $0.203 \times 10^{-2} \text{ (1/kPa)}$
C = $0.2 \times 10^3 \text{ (kPa)}$	$R_0 = 2.5$
W = -0.00267	D = $-0.12 \times 10^{-2} \text{ (1/kPa)}$
GI = $0.09489 \times 10^5 \text{ (kPa)}$	KI = $0.33333 \times 10^5 \text{ (kPa)}$
<b>4. Fluid (water)</b>	
Compressibility of water, c	1439.0 (m/sec)
Density of water, $\rho_f$	$1000 \text{ (kg/m}^3)$

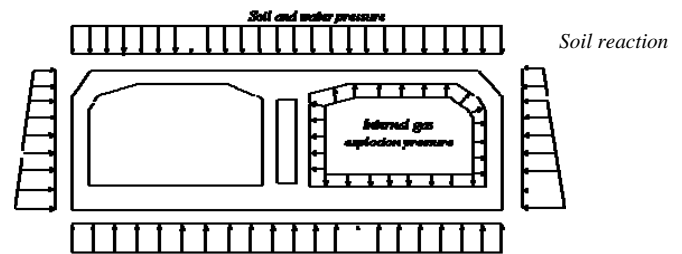


Figure (11): Tunnel load cases: (1) dead weight, (2) sand and water and (3) internal pressure.

For the internal pressure, the approximate pressure time-history, shown in Figure (12), is used under the following assumptions:

- (1) the full length of the tunnel is entirely filled with gas, (2) the detonation commences at the center of the tunnel, (3) the tunnel section to be analyzed is located at the quarter point, i.e. at a distance of about 80 m from the tunnel exit, (4) the shock wave velocity is  $2000 \text{ m/sec}$  and (5) the velocity of the depressurization wave is half that value, i.e.  $1000 \text{ m/sec}$ , because depressurization is associated with fluid flow.

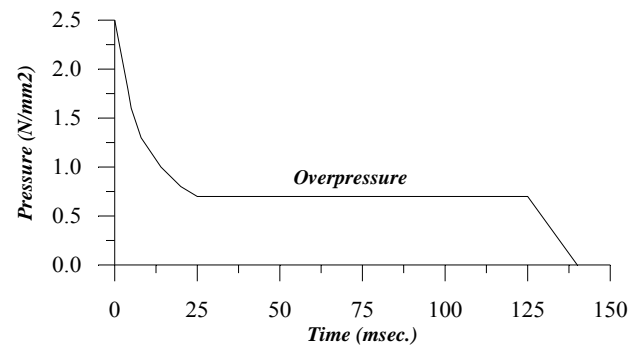


Figure (12): Pressure time history for an internal gas explosion (Mier, [185]).

Due to the fact that the connection of the tunnel roof to the intermediate wall is the most critical feature, the analyses are confined to the shaded part shown in Figure (10).

## Linear analysis

This analysis is performed for three cases: (1) Reinforced concrete tunnel roof model only (*i.e.*, *uncoupled solution*) with weight of 2-m sand and 10-m water above as lumped masses at the nodes along the upper boundary of the tunnel roof elements. (2) Reinforced concrete tunnel roof plus 2-m sand above as finite elements (*i.e.*, *class II coupling*) with 10-m water applied as lumped masses at the nodes along the upper boundary of the soil elements. (3) Full finite element model of reinforced concrete tunnel roof plus 2-m sand and 10-m water as finite elements (*i.e.*, *class I plus II couplings*). The finite element meshes for the three cases are shown in Figure (13a, b and c), respectively.

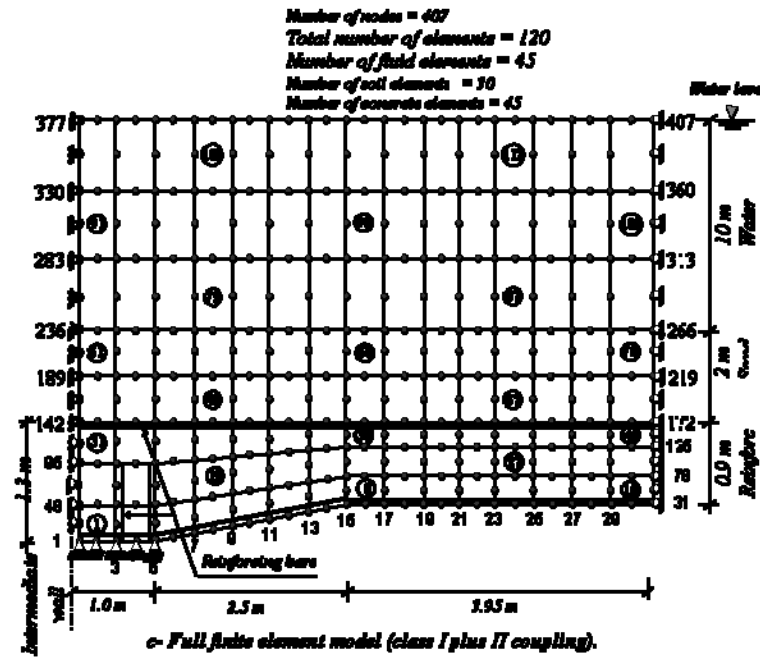
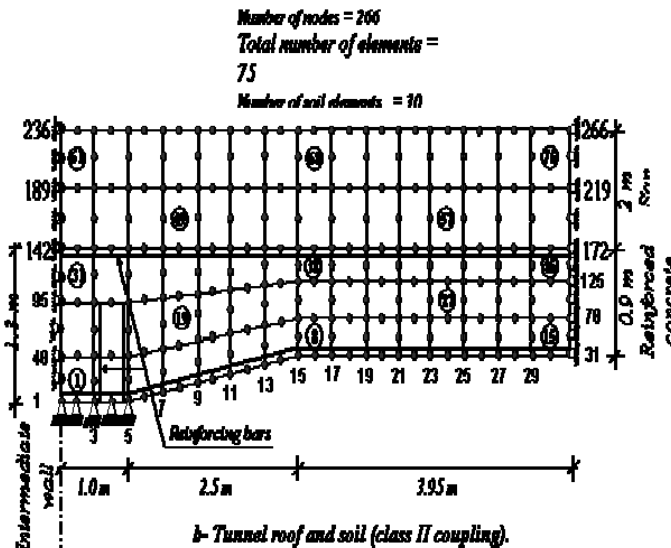
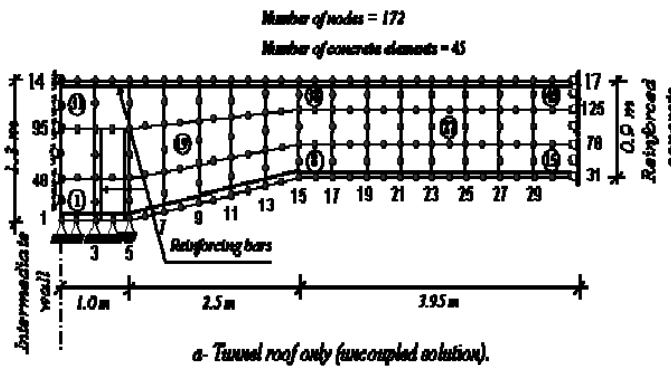


Figure (13): Finite element meshes used in the analyses.

In each case, 10% damping is used for the two frequencies  $\omega_1 = 125$  Rad/sec and  $\omega_2 = 1250$  Rad/sec. This is equivalent to the Rayleigh damping parameters  $\alpha = 22.7$  and  $\beta = 0.000145$ . Each material (reinforced concrete, sand or water) is represented by eight-noded plane-strain isoparametric elements that are numerically integrated with 3x3 Gauss points. The reinforcement is represented by the *embedded bar simulation* with two nodes connected to the nodes of the 8-noded basic (concrete) elements.

The results of the linear analyses at nodal point 31 are shown in Figure (14). It is clear that for the uncoupled solution, the deflection oscillates and reaches peak amplitude of 150 mm during the earlier time steps then reduces with the progress of time. Whereas, in case of a tunnel roof plus soil, the deflection values show a change in phase and amplitude especially at earlier time steps due to the significant effect of class II coupling and the different modeling of soil behavior. This means that the simulation of soil above the tunnel roof as lumped masses give errors in phase and amplitudes of the computed displacements. At the beginning of shock, the deflection reaches a value of 63 mm. After that, the deflection reduces with the progress of time. This behavior is attributed to the role of water which shares the solid particles in carrying the applied load at the earlier stages, then, diminishes as the excess pore water pressure dissipates with the progress of time, since drainage is allowed through boundary conditions. Figure (14) also shows that, with class I plus II couplings, there is a slight change in phase and amplitude of the deflection values in comparison with those of class II coupling only. This may be attributed to the limited coupling effects at only the upper boundary of soil elements. Therefore, the simulation of water as lumped masses above the soil elements gives small errors in phase and amplitude of deflection values

for linear analyses.

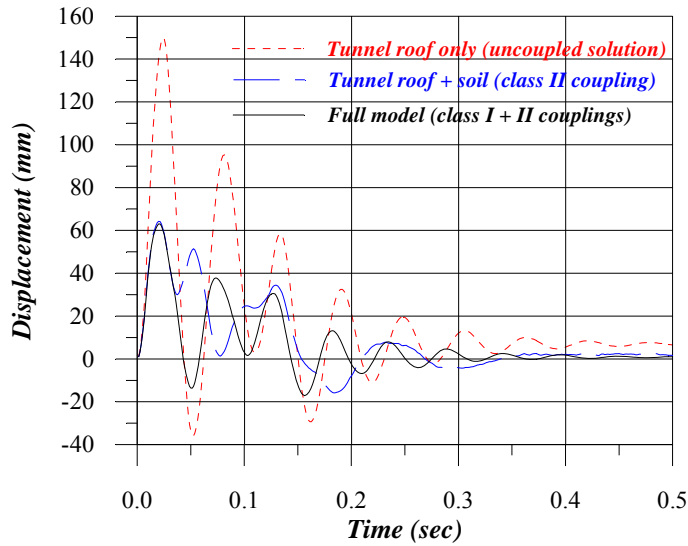


Figure (14): Midspan deflection of the tunnel roof at nodal point 31 (linear analysis).

**Nonlinear analysis**

Again, this analysis involves the same three cases analyzed in the linear analysis. Here, the cap model is used as a constitutive relation for sand and the elasto-plastic Druker-Prager model with Kupfer’s and Gerstle [42] criterion is adopted for the reinforced concrete tunnel. The results of these analyses for the three cases are shown in Figure (15) as a midspan deflection time-history of the tunnel roof at nodal point 31.

It is noticed that, for the uncoupled solution, the displacement increases with the progress of time with a maximum displacement of 90 mm at 0.5 second. Whereas, with class II coupling, the displacement sharply increases at the beginning, as indicated by the steeper slope of the displacement-time history curve in Figure (15), then follows by a gradual increase of displacements due to all gravity loads exerted by soil and water. However, the rate of displacement increase becomes small at larger time steps with a maximum displacement of 312.5 mm at 0.5 second. This can be attributed to the modeling of soil above the tunnel roof as finite elements instead of added masses (used in the case of uncoupled solution) at the upper boundary of the reinforced concrete tunnel roof as well as the effect of the excess pore water pressure generated through class II coupling.

Figure (15) also shows the results of analysis for the full model with class I + II couplings. It is noticed that the response only at the beginning is similar to that of class II coupling; however, the rate of displacement increase becomes small at larger time steps with a maximum displacement of 266 mm at 0.5 second. The gap between the linear and nonlinear analyses results (Figures 14 and 15) is due to the flow of the yielded materials.

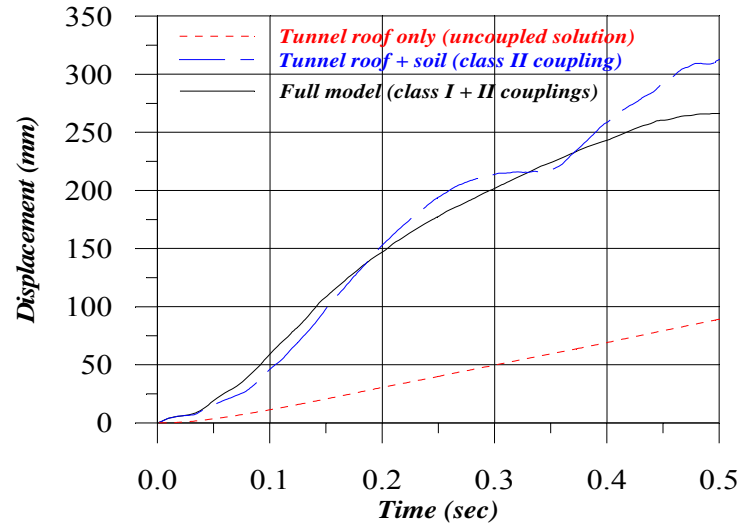


Figure (15): Midspan deflection of the tunnel roof at nodal point 31 (nonlinear analysis).

The steel stresses in the two vertical reinforcing bars, which tie the roof slab into the vertical walls are plotted as a function of time in Figure (16a, b and c) for uncoupled, class II coupling and full model analysis, respectively. It can be noticed that while these two bars provide a fixed end moment, the tensile stress in each of them builds up. Therefore, they cannot prevent the vertical pressure from lifting the roof off its supports. The steel strains in these left and right bars after 0.1 (i.e., the period for the applied internal gas explosion pressure) and 0.5 seconds are listed in Table (2). Also, it is important to mention that after 0.1 second, all of the steel integration points ( $3 \times 3 \times 34 = 306$ ) are yielded, which can only be interpreted as failure.

Table (2): Tensile strains in left and right vertical bars.

Case number	Time (second)	Tensile strain	
		Left bar	Right bar
1. Tunnel roof only.	0.1	0.00003	0.25970
	0.5	0.13430	-----
2. Tunnel roof + soil.	0.1	0.00000	0.00188
	0.5	-0.00024	0.01623
3. Full model.	0.1	0.03982	0.00994
	0.5	0.00000	0.01871

The concrete stresses are not critical at any time of the analysis as shown in Figures (17, 18 and 19) for the three cases considered at several time intervals. The combination of flexure with axial tension compelled the reinforcing steel to

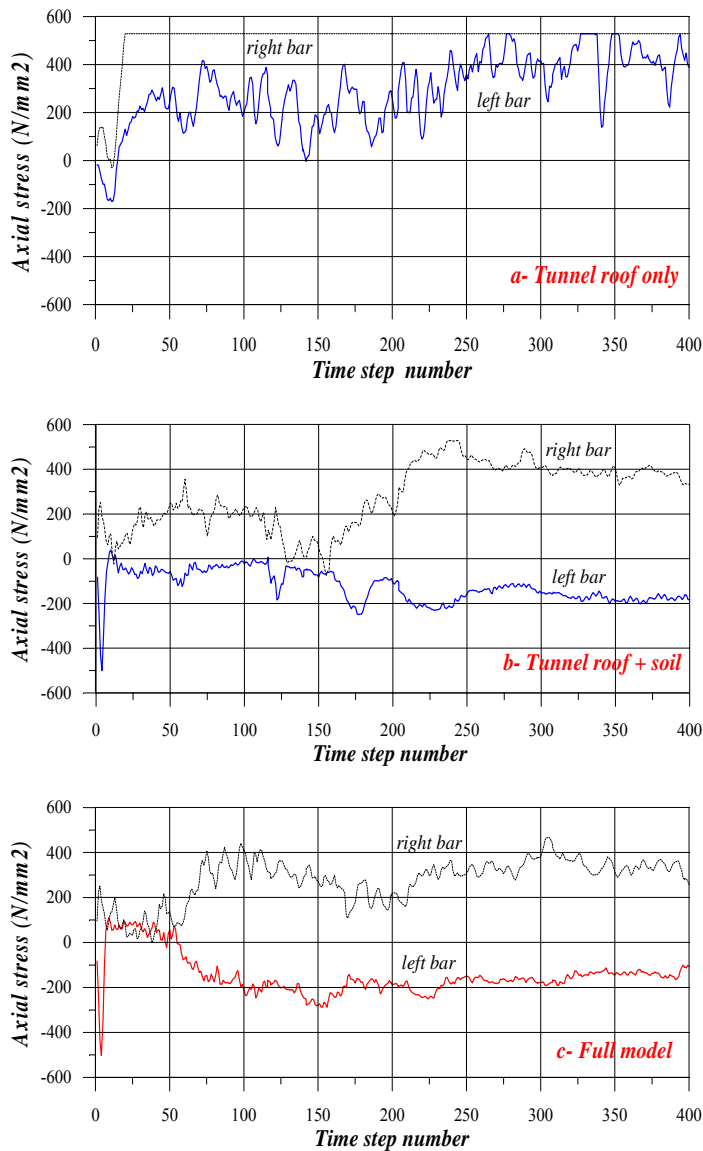


Figure (16): Time histories of stresses in vertical reinforcing bars (nonlinear analysis).

resist most of the load. The stress contours show that at earlier stages of load, (at time = 0.00125 second) show a uniform spacing of stress contours across the depth of the tunnel roof indicates an approximately linear variation with neutral axis at about half the depth from the compression face. This is valid for all types of analyses. Whereas, for the uncoupled solution, after 0.1 second (i.e., the period for the applied internal gas explosion pressure) the concentration of compressive stresses causes a fluctuation of the neutral axis position and the tensile stresses are gradually increased above the steel bars levels due to cracked zones (up to 76 integration points cracked after 0.1 second).

However, for other types of analyses, the tensile stresses gradually disappear after 0.1 second due to cracking of concrete at some integration points (up to 63-67 integration points cracked during time step 80, i.e., after 0.1 second, yet the solution converged almost at each time step within five iterations to the specified energy tolerance of 0.001).

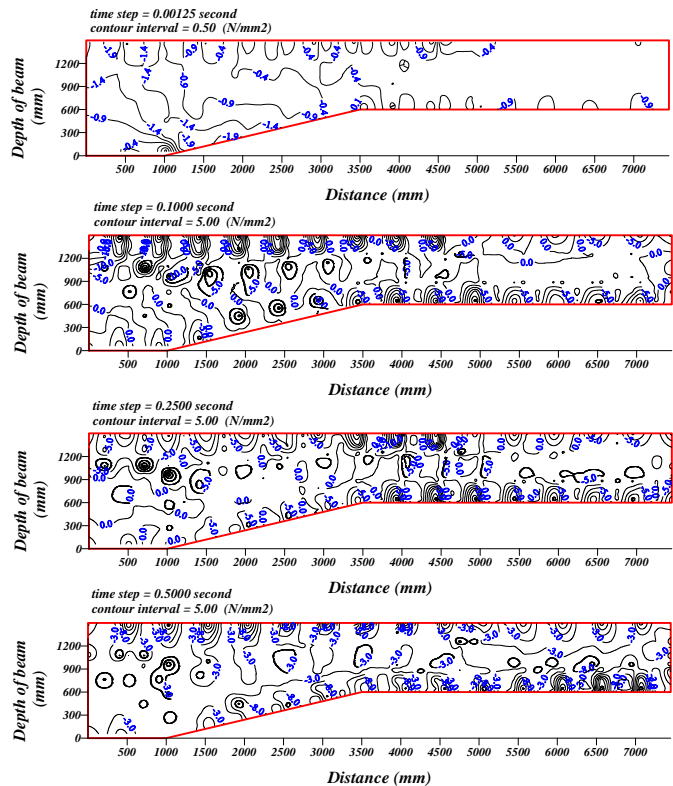


Figure (17): Contours of x-concrete stress for tunnel roof only (uncoupled solution).

Also, a pronounced thrust arch is observed which equilibrates the mid-span tensile reinforcement. The number of cracked integration points after 0.5 second is 87, 96 and 84 for the three cases analyzed, respectively. Finally, as the total number of concrete integration points is  $(3 \times 3 \times 45 = 405)$ , it can be concluded that the tunnel roof is not likely to survive a gas explosion load of the kind shown in Figure (10.42).

## CONCLUSIONS

The developed computer code and the solution algorithms based on the *pressure formulation* for modeling of the free fluid and on the *u-p formulation* for predicting the coupled behavior of soils are found to be efficient for the problem of an internal gas explosion in a tunnel solved herein. The coupling has a significant effect on the response indicated by the lower values of the horizontal surface displacement compared with those of uncoupled analysis. This is due to the role of water in the pores which shares the solid in carrying the applied load at the earlier stages, then, diminishes as the excess pore water pressure is dissipated with the progress of time. The cap plasticity model can successfully simulate the response of dry or saturated sands under dynamic loads. However, the model is very sensitive to the maximum volumetric plastic strain that the material experiences. A slight change in its value may cause large changes in the pore

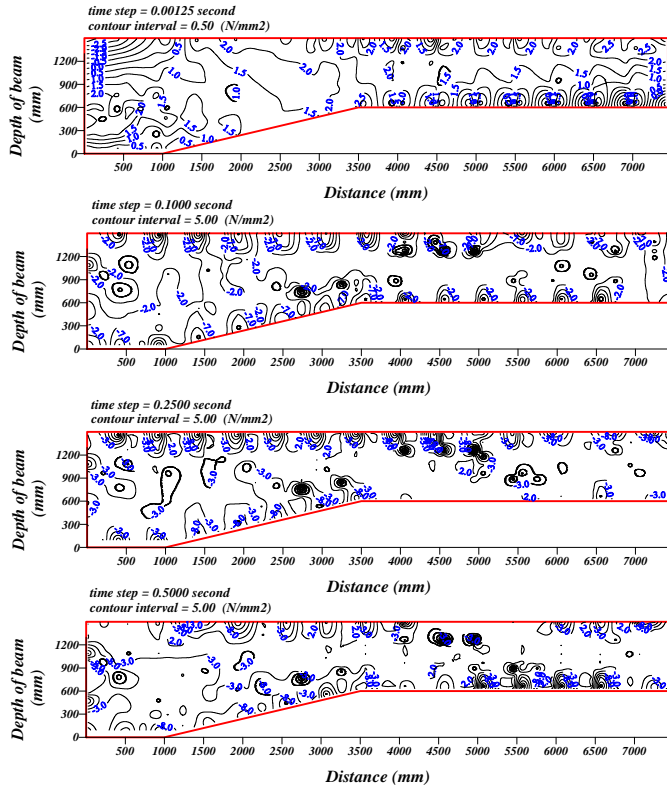


Figure (18): Contours of x- concrete stress for tunnel roof + soil (class II coupling).

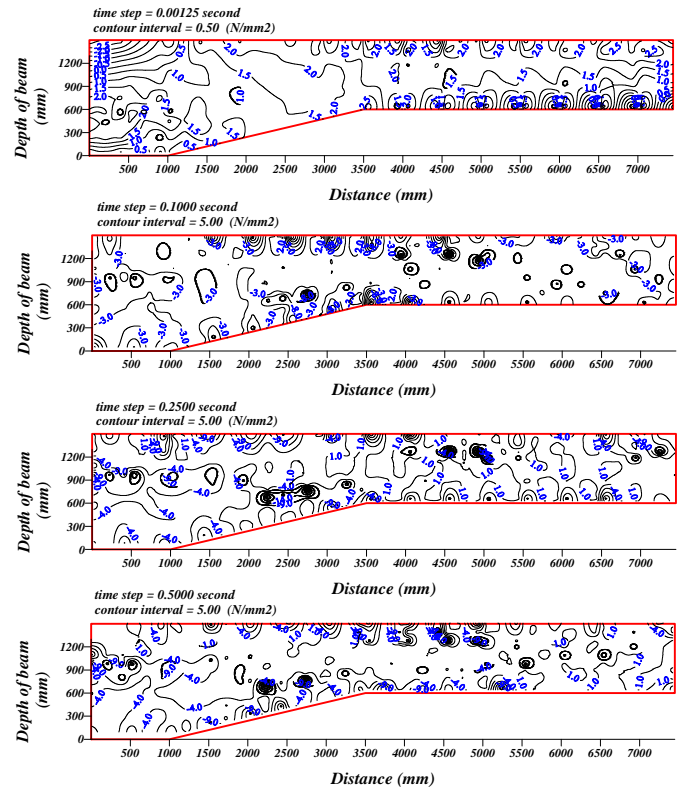


Figure (19): Contours of x-concrete stress for full model (class I + II couplings).

pressures. Thus, care should be taken in the selection of the cap model parameters. The behavior of a reinforced concrete tunnel roof can be well predicted by the elasto-plastic Druker-Prager model with Kupfer's and Gerstle criterion. In particular, the midspan deflection-time history and location and direction of tensile cracking are determined with sufficient accuracy.

## REFERENCES

Abboud, N. N., and Pinsky, P. M., (1988), "Mixed Variational Principle for the Structure-Exterior Fluid Interaction Problem", Proceedings of the International Symposium on Flow-Induced Vibration and Noise: Acoustic Phenomena and Interaction in Shear Flows over Compliant and Vibrating Surfaces, ASME, New York, pp. 137-148.

Abdul-Aziz, R. A., (2002), "Dynamic Analysis of Reinforced Concrete Members by Bounding Surface Plasticity Model", Ph.D. Thesis, University of Baghdad, Iraq.

Aboim, C. A., and Roth, W. H., (1982), "Bounding Surface Plasticity Applied to Cyclic Loading of Sand", International Symposium on Numerical Models in Geomechanics, Zurich, pp. 65-72.

Aggour, M. S., Tawfiq, K. S., and Amini, F., (1987), "Effect of Frequency Content on Dynamic Properties of Cohesive Soils", Soil Dynamics and Liquefaction, Developments in Soil Mechanics 42, Elsevier.

Al-Nu'aimy, R.M.S., (2004), "Non-Linear Analysis of Coupled-Soil-Fluid-Structure Interaction Under Dynamic Loading", Department of Civil Engineering, University of Baghdad, Iraq.

Altaee, A., Evgin, E., and Fellenius, B. H., (1992), "Finite Element Validation of A Bounding Surface Plasticity Model", Computers and Structures, Volume 42, No.5, pp. 825-832.

Aslam, M., (1981), "Finite Element Analysis of Earthquake-Induced Sloshing in Axi-symmetric Tanks", International Journal of Numerical Methods in Engineering, Volume 17, pp. 159-170.

Ayvazyan, H., Dede M., Dobbs N., Whitney M., Bowles P., Baker W., and Caltagirone J. P., (1986), "Structures to Resist the Effects of Accidental Explosions", Volume II, Blast, Fragment, and Shock Loads", U.S. Army Special Report, Dover, New Jersey.

- Barbat, A. H., (1984), "Seismic Soil-Structure-Fluid Interaction Analysis", Chapter 12, Numerical Methods in Coupled Systems, edited by R. W. Lewis, P. Bettes, and E. Hinton, John Wiley & Sons, pp. 353-386.
- Bardet, J. P., (1983), "Application of Plasticity Theory to Sand Behaviour, a New Sand Model", Thesis Presented to the California Institute of Technology, at Pasadena, California, in Partial Fulfillment of the Requirements for the Degree of Doctor of Philosophy.
- Bardet, J. P., (1985), "Application of Bounding Surface Plasticity to Cyclic Sand Behaviour", Second International Conference on Soil Dynamics and Earthquake Engineering, Springer and Verlag, Session 2, pp. 3-16.
- Bardet, J. P., (1986a), "Bounding Surface Plasticity Model for Sands", Journal of Engineering Mechanics Division, ASCE, Volume 112, No. 11, November, Paper 21045, pp. 1198-1217.
- Bardet, J. P., (1986b), "Modelling of Sand Behaviour with Bounding Surface Plasticity", Second International Symposium on Numerical Models in Geomechanics, Ghent, pp. 79-90.
- Bathe, K., and Hahn, W., (1979), "On Transient Analysis of Fluid-Structure Systems", Journal of Computers and Structures, Volume 10, pp. 383-391.
- Belytschko, T., (1980), "Fluid-Structure Interaction", Journal of Computers and Structures, Volume 12, pp. 459-469.
- Belytschko, T., and Kennedy, J., (1976), "A Fluid-Structure Finite Element Method For the Analysis of Reactor Safety Problems", Journal of Nuclear Engineering and Design, Volume 38, pp. 71-81.
- Belytschko, T., and Kennedy, J., (1978), "Computer Models For Subassembly Simulation", Journal of Nuclear Engineering and Design, Volume 49, pp. 17-38.
- Biot, M. A., (1941), "General Theory for Three-Dimensional Consolidation", Journal of Applied Physics, Volume 12, No. 2, pp. 155-164.
- Biot, M. A., (1955), "Theory of Elasticity and Consolidation for a Porous Anisotropic Solid", Journal of Applied Physics, Volume 26, pp. 182-185.
- Borm, G. W., (1977), "Rock Dynamics and Geophysical Aspects", Proceedings of Dynamical Methods in Soil and Rock Mechanics", Volume 3.
- Chang, C. T., Hinton, E., and Zienkiewicz, O. C., (1984), "Non-linear Response of Structure-Fluid-Foundation Systems to Earthquake Excitation", Chapter 11, Numerical Methods In Offshore Engineering, pp. 341-359.
- Chen, W. F., (1982), "Plasticity in Reinforced Concrete", McGraw-Hill Book Company.
- Chen, W. F., and McCarron, W. O., (1983), "Modelling of Soils and Rocks Based on Concepts of Plasticity", Proceedings of the Symposium on Recent Developments in Laboratory and Field Tests and Analysis of Geotechnical Problems, Asian Institute of Technology, Bangkok, Thailand, pp.467-510.
- Chopra, A. K., and Chakrabarti, P., (1981), "Earthquake Analysis of Concrete Gravity Dams, Including Foundation Rock Interaction", Earthquake Engineering and Structural Dynamics, Volume 9, pp. 363-383.
- Chopra, A., Wilson, E., and Farhoomand, I., (1969), "Earthquake Analysis of Reservoir-Dam Systems", Proceedings of the 4<sup>th</sup> World Conference on Earthquake Engineering, Santiago, Chile.
- Chu, L. L., Askar, A., and Cakmak, A. S., (1981), "An Approximate Method for Soil-Structure Interaction for SH-Waves-The Born Approximation", Journal of Earthquake Engineering and Structural Dynamics, Volume 9, pp. 205-219.
- DiMaggio, F. L., and Sandler, I. S., (1971), "Material Model for Granular Soils", Journal of Engineering Mechanics Division, ASCE, Volume 97, No. EM3, Proceedings Paper 8212, pp. 935-950.
- Donea, J., (1980), "Finite Element Analysis of Transient Dynamic Fluid-Structure Interaction", Advanced Structural Dynamics, pp. 255-290.
- Everstine, G. C., (1981), "A Symmetric Potential Formulation For Fluid-Structure Interaction", Journal of Sound and Vibration, Volume 79, pp. 157-160.
- Everstine, G. C., and Henderson, F. M., (1990), "Coupled Finite Element Boundary Element Approach for Fluid Structure Interaction", Journal of the Acoustical Society of America, Volume 87, No. 5, pp. 1938-1947.
- Everstine, G. C., Marcus, M. S., and Quezon, A. J., (1983), "Finite Element Analysis of Fluid-Filled Elastic Piping System", Proceedings of the Eleventh NASTRAN Users' Colloquium, NASA Conference Publication, pp. 141-160.
- Fertis, D. G., (1973), "Dynamics and Vibrations of Structures", John Wiley and Sons.
- Guan, F., and Moore, I. D., (1997), "New Techniques for Modelling Reservoir-Dam and Foundation-Dam Interaction", Journal of Soil Dynamics and Earthquake Engineering, Volume 16, pp. 285-293.
- Hamdi, M., Ousset, Y., and Verchery, G., (1978), "A Displacement Method For the Analysis of Vibrations of Coupled Fluid-Structure Systems", International Journal for Numerical Methods in Engineering, Volume 13, pp. 139-150.

- Hashiguchi, K., and Ueno, M., (1977), "Elasto-Plastic Constitutive Laws of Granular Materials", Preprints of Specialty Session 9—Constitutive Equations of Soils, Ninth International Conference on Soil Mechanics and Foundation Engineering, Tokyo, Japan, pp.72-82.
- Hill, R., (1950), "The Mathematical Theory of Plasticity", Oxford University Press, London.
- Hinton E., (1988), "Numerical Methods and Software for Dynamic Analysis of Plates and Shells", Pineridge Press, Swansea, U.K.
- Johnson, W., (1984), "Aspects of Damage to Buildings from Uncased Explosives", Mechanics of Material Behavior, Edited by G. H., Dvorak and R. T., Shield.
- Joseph, H. S., (1997), "Fluid Mechanics", Springer, Chapters 2 and 3.
- Kinney, G. F., and K. J. Graham, (1985), "Explosive Shocks in Air", Springer-Verlag.
- Kock, E., and Olson, L., (1991), "Fluid Structure Interaction Analysis by the Finite Element Method- a Variational Approach", International Journal for Numerical Methods in Engineering, Volume 31, No. 3, March, pp. 463-491.
- Kupfer, H. B., and Gerstle, K. H., (1973), "Behaviour of Concrete Under Biaxial Stresses", Journal of the Engineering Mechanics Division, ASCE. Volume 99, No. EM4, August, pp. 852-866.
- Leger, P. and Katsouli, M., (1989), "Seismic Stability of Concrete Gravity Dams", Earthquake Engineering and Structural Dynamics, Volume 18, pp. 889-902.
- Li, X. and Zienkiewicz, O. C., (1992), "Multiphase Flow In Deforming Porous Media and Finite Element Solutions", Journal of Computers and Structures, Volume 45, No. 2, pp. 211-227.
- Liu, W. K., and Uras, R. A., (1988), "Variational Approach to Fluid-Structure Interaction with Sloshing", Journal of Nuclear Engineering and Design, Volume 106, No. 1, February, pp. 69-85.
- Luke, I., (1967), "A Variational Principle for a Fluid With a Free Surface", Journal of Fluid Mechanics, Volume 27, pp. 395-397.
- Mahmood, M. N., (1994), "Investigation of Post Cracking Behaviour of Reinforced Concrete Girder Bridges", Ph.D. Thesis, University of Roorkee, India, 247 pps.
- Mier, J. G. M., (1987), "Examples of Non-Linear Analysis of reinforced Concrete Structures with DIANA", HERON, Volume 32, No. 3, pp. 124-147.
- McCarron, W. O., and Chen, W. F., (1987), "A Mapped Plasticity Model Applied to Boston Blue Clay", Canadian Geotechnical Journal, Volume 24, No. 4, pp. 630-644.
- Miles, J., (1977), "Hamilton's Principle for Surface Waves", Journal of Fluid Mechanics, Volume 83, pp. 153-158.
- Morand, H., and Ohayon, R., (1979), "Substructure Variational Analysis of the Vibrations of Coupled Fluid-Structure Systems. Finite Element Results", International Journal of Numerical methods in Engineering, Volume 14, pp. 741-755.
- Naylor, D. J., (1974), "Stresses In Nearly Incompressible Materials By Finite Elements With Application To The Calculation Of Excess Pore Pressures", International Journal For Numerical Methods In Engineering, Volume 8, pp. 443-460.
- Nitikitpaiboon, C., and Bathe K. J., (1993), "An Arbitrary Lagrangian-Eulerian Velocity Potential Formulation for Fluid Structure Interaction", Journal of Computers and Structures, Volume 47, No. 4-5, June, pp. 871-891.
- Nogami, T., and Kazama, M., (1997), "Thin Layer Element Method for Dynamic Soil-Structure Interaction Analysis of Axi-Symmetric Structure in Submerged Soil", Journal of Soil Dynamics and Earthquake Engineering, Volume 16, pp. 337-351.
- Norris C. H., Hanssen R. J., Holley M. J., Bigs J. M., Namyet S., and Minami J. K., (1959), "Structural Design for Dynamic Loads", McGraw-Hill Book Company.
- Ohayon, R., and Valid, R., (1981), "True Symmetric Formulation of Free Vibration of Fluid-Structure Interaction-Applications and Extensions", Proceedings of the International Conference of Numerical Methods for Coupled Problems, University College, Swansea, September.
- Oka, F., and Washizu, H., (1981), "Constitutive Equations for Sands and Overconsolidated Clays Under Dynamic Loads Based on Elasto-Plasticity", International Conference on Recent Advances in Geotechnical Earthquake Engineering and Soil Dynamics, April 26-May 3, University of Missouri-Rolla, Rolla, Missouri, pp. 71-74.
- Olson, L. G., and Bathe, K. J., (1983), "A Study of Displacement-Based Fluid Finite Elements For Calculating Frequencies of Fluid and Fluid-Structure Systems", Journal of Nuclear Engineering and Design, Volume 76, pp. 137-151.
- Olson, L. G., and Bathe, K. J., (1985), "An Infinite Element for Analysis of Transient Fluid-Structure Interaction", Journal of Engineering with Computers, Volume 2, December, pp. 319-329.
- Owen, D. R. J., and Hinton, E., (1980), "Finite Elements in Plasticity-Theory and Practice", Pineridge Press Ltd., Swansea.

- Park, K.C., and Felippa, C. A., (1984), "Recent Developments in Coupled Field Analysis Methods", Chapter 11 in *Numerical Methods in Coupled Systems* (edited by R. W. Lewis, P. Bettess, and E. Hinton, John Wiley and Sons), pp. 327-351.
- Pastor, M., Li, T., and Merodo J. A. F., (1997), "Stabilized Finite Elements for Harmonic Soil Dynamics Problems Near the Undrained-Incompressible Limit", *Journal of Soil Dynamics and Earthquake Engineering*, Volume 16, pp. 161-171.
- Pastor, M., Zienkiewicz, O. C., and Leung, K. H., (1985), "Simple Model for Transient Soil Loading in Earthquake Analysis. II. Non-Associative Models for Sands", *International Journal for Numerical and Analytical Methods in Geomechanics*, Volume 9, pp. 453-476.
- Paul, D. K., (1982), "Efficient Dynamic Solutions for Single and Coupled Multiple Field Problems", Ph.D. Thesis, University College, Swansea.
- Pinsky, P. M., and Abboud, N. N., (1989), "Two Mixed Variational Principles for Exterior Fluid Structure Interaction Problems", *Journal of Computers and Structures*, Volume 33, No. 3, pp. 621-635.
- Sandler I. S., DiMaggio F. L. and Baladi G. Y., (1976), "Generalized Cap Model for Geological Materials", *ASCE* Volume 102, No. GT7.
- Seliger, R., and Whitham, G., (1968), "Variational Principles in Continuum Mechanics", *Proceedings of the Royal Society, Series A*, Volume 305, pp. 1-25.
- Serrin, J., (1959), "Mathematical Principles of Classical Fluid Mechanics", *Encyclopedia of Physics*, Volume 8, Springer-Verlag, Berlin, pp. 125-263.
- Shawky, A. and Maekawa, K., (1996), "Nonlinear Response of Underground RC Structures Under Shear", *Journal of Materials, Concrete Structures and Pavements*, JSCE, Volume 31, 538, pp. 195-206.
- Shukr, W. G., (1999), "Three-Dimensional Non-Linear Finite Element Analysis of High Strength Reinforced Concrete Panels under Combined Loadings", M.Sc. Thesis, Department of Building and Construction, University of Technology, Iraq.
- Simon, B. R., Wu, J. S. S., Zienkiewicz, O. C. and Paul, D. K., (1986), "Evaluation of  $u-w$  and  $u-\pi$  Finite Element Methods for the Dynamic Response of Saturated Porous Media Using One-Dimensional Models", *International Journal for Numerical and Analytical Methods in Geomechanics*, Volume 10, pp.461-482.
- Spyrakos, C. C., and Xu, C., (1997), "Soil-Structure-Water Interaction of Intake-Outlet Towers Allowed to Uplift", *Journal of Soil Dynamics and Earthquake Engineering*, Volume 16, pp. 151-159.
- Thannon, A. Y., (1988), "Ultimate Load Analysis of Reinforced Concrete Stiffened Shells and Folded Slabs Used in Architectural Structures", Ph.D. Thesis C/ Ph/ 109/ 88, University of Wales, Swansea.
- Wang, Z. L., Dafalias, Y. F., and Shen, C. K., (1990), "Bounding Surface Hypoplasticity Model for Sands", *Journal of Engineering Mechanics Division, ASCE*, Volume 116, No. 5, May, Paper 24615, pp. 983-1001.
- Wilson, E., and Khalvati, M., (1983), "Finite Elements for the Dynamic Analysis of Fluid-Solid Systems", *International Journal of Numerical Methods in Engineering*, Volume 19, pp. 1657-1668.
- Wolf, J., and Darbre, G., (1986), "Non-linear Soil-Structure Interaction Analysis Based on the Boundary-Element Method in Time Domain with Application to Embedded Foundation", *Journal of Earthquake Engineering and Structural Dynamics*, Volume 14, pp. 83-101.
- Yang, Z., (1996), "Finite Element Simulation of Buried Shelters to Blast Loadings", *Journal of Finite Elements in Analysis and Design*, Volume 24, pp.113-132.
- Zaman, M. M., Desai, C. S. and Drumm, E. C., (1984), "Interface Model for Dynamic Soil-Structure Interaction", *Journal of Geotechnical Engineering*, Volume 110, No. 9, pp. 1257-1272.
- Zeng, X. G., Bielak J., and MacCamy, R. C., (1992), "Stable Variational Coupling Method for Fluid-Structure Interaction in Semi-infinite Media", *Journal of Vibration and Acoustics, Transactions of the ASME*, Volume 114, No. 3, July, pp. 387-396.
- Zienkiewicz, O. C., (1984), "Coupled Problems and Their Numerical Solution", Chapter One, *Numerical Methods in Coupled Systems* (edited by R. W. Lewis, P. Bettess, and E. Hinton, John Wiley & Sons), pp. 319-350.
- Zienkiewicz, O. C., and Bettess, P., (1978), "Fluid-Structure Dynamic Interaction and Wave Forces. An introduction of Numerical Treatment", *International Journal of Numerical Methods in Engineering*, Volume 13, pp. 1-16.
- Zienkiewicz, O. C., and Bettess, P., (1982), "Soils and other Saturated Media under Transient, Dynamic Conditions: General formulation and the Validity of the Various Simplifying Assumptions", Chapter One in *Soil Mechanics: Transient and Cyclic Loads*, Edited by G. N. Pande and O. C. Zienkiewicz, Wiley New York, pp.1-16.
- Zienkiewicz, O. C., Chan, C. T., and Bettess, P., (1980), "Drained, Undrained, Consolidating Dynamic Behaviour Assumptions in Soils", *Geotechnique*, Volume 30, pp.385-395.
- Zienkiewicz, O. C., and Newton, R., (1969), "Coupled Vibrations of a Structure Submerged in a Compressible Fluid", *Symposium on Finite Element Techniques*, Stuttgart.

Zienkiewicz, O. C., and Shiomi, T., (1984), "Dynamic Behaviour of Saturated Porous Media: The Generalized Biot Formulation and Its Numerical Solution", Journal of Numerical Analytical Methods in Geomechanics, Volume 8, pp.71-96.

Zienkiewicz, O. C. and Taylor R. L., (1991), "The Finite Element Method", Fourth. Edition, McGraw-Hill Book Co. (UK), Volume 2, Chapter 11, Coupled Systems, pp.404-429.

Zienkiewicz, O. C., Bettess, P. and Kelly, D. W., (1978), "The Finite Element Method for Determining Fluid Loading on Rigid Structures, Two-and Three Dimensional Formulations", Numerical Methods in Offshore Engineering, Chapter Four, edited by O. C. Zienkiewicz, et al., John Wiley and Sons, pp. 141-184.

Zienkiewicz, O. C., Chan, A. H. C., Pastor, M., Paul, D. K., and Shiomi, T., (1990), "Static and Dynamic Behaviour of Soils: A Rational Approach to Quantitative Solutions. I Fully Saturated Problems", Proceedings of the Royal Society of London, Volume 429, pp.285-309.

Zienkiewicz, O. C., Pastor, M., Chan, A. H. C., and Xie, Y. M., (1991), "Computational Approaches to the Dynamics and Statics of Saturated and Unsaturated Soils", In Advanced Geotechnical Analysis, Eds. P. K. Banerjee and R. Butterfield, Elsevier, Oxford, Chapter One, pp.1-46.

Zienkiewicz, O. C., Xie, Y. M., Schrefler, B. A., Ledesma, A., and Bicanic, N., (1990), "Static and Dynamic Behaviour of Soils: A Rational Approach to Quantitative Solutions. II Semi-Saturated Problems", Proceedings of the Royal Society of London, Volume 429, pp.311-321.

LIST OF SYMBOLS:

$\underline{b}$  = Displacement of fluid relative to the solid skeleton.

$\underline{B}$  = Strain –displacement matrix.

$c$  = Speed of sound.

$\underline{C}_s$  = Rayleigh damping matrix.

$\underline{C}_f$  = Compressibility matrix.

$C_{ijkl}$  = Components of the elasticity tensor.

$D_t$  = Constitutive matrix.

$E$  = Modulus of elasticity specified  $\bar{E}$  = Adopted modulus of elasticity in analysis.

$g$  = Gravitational acceleration.

$G$  = Shear modulus.

$\hat{i}$ ,  $\hat{j}$ ,  $\hat{k}$  = Unit vectors in x, y and z directions, respectively.

$k$  = Permeability coefficient.

$K$  = Bulk modulus .

$\underline{K}_s$  = Stiffness matrix.

$\underline{K}_f$  = Flow matrix.

$K_f$  = Bulk modulus of the fluid.

$K_s$  = Bulk modulus of the solid phase.

$K_T$  = Total bulk modulus of the solid skeleton.

$\underline{L}$  = Coupling matrix .

$L$  = Loading index.

$\underline{L}_{ij}$  = Loading direction.

$\underline{M}_s$  = Solid skelton mass matrix.

$\underline{M}_f$  = Fluid mass matrix.

$n$  = Porosity.

$\mathbf{n}$  = the direction of the unit normal at the radiating boundary.

$\underline{N}_p$  = Shape functions for pore pressure.

$\underline{N}_u$  = Shape functions for solid skeleton displacements.

$P_f$  = Mass density.

$P$  = Pressure above the hydrostatic value.

$P_d^h$  = Hydrodynamic pressure.

$P_s$  = Static pressure.

$t$  = Surface traction.

$T$  = Time.

$\underline{u}$  = Solid phase translation.

$\dot{u}_x$ ,  $\dot{u}_y$  and  $\dot{u}_z$  = Velocity of solid phase components in x, y and z directions, respectively.

$\underline{W}$  = Fluid velocity.

$Y$  = Rise from dam base.

$\alpha$  and  $\beta$  are Rayleigh damping constants.

$\alpha_c = 1 - K_T / K_S$ .

$\underline{\epsilon}^0$  = Autogenous strains.

$\epsilon_{ij}$  = Strains due to stresses and the superscripts.

$\Gamma$  = Boundary surface.

$\mu'$  = The dynamic viscosity of fluid.

$\rho$  = Solid phase density.

$\rho_f$  = Fluid density.

$\underline{\sigma}_{ij}$  = Stress tensor.

$\Omega$  = The domain.

A superposed dot indicates the rate.